Operando Spectro-electrochemical investigations of Pt and Pt-alloys as fuel cell catalysts

Nagra, H.J.

Chapter 4

The potential-dependent structure of Pt_3Ni alloy electrocatalysts and its effect on electrocatalytic activity

Abstract

The distribution of elements within alloy nanoparticles is a critical parameter for their electrocatalytic performance. Here, we use the case of a Pt_3Ni alloy to show that this elemental distribution can dynamically respond to the applied potential, leading to strongly potential-dependent catalytic properties. Starting from the $PtNi_x$ core and a Pt shell (formed by Pt-Ni alloys in acidic electrolyte due to Ni leaching), our electrochemical X-ray photoelectron spectroscopy measurements show that the Ni atoms can be reversibly moved between the core of the particles and the near-surface region using the applied potential. Through potential jump measurements, we show that this Ni migration modulates the hydrogen evolution reaction activity of the particles by over 30%. These observations highlight the potential of incorporating in situ restructuring of alloys as the final step in electrocatalyst design.

This Chapter has been submitted for publication:

Javed, H.; Kolmeijer, K.; Deka, N.; Sandhya, A. L. M.; Khalakhan, I.; Mom, R. V. The Potential-Dependent Structure of Pt3Ni Alloy Electrocatalysts and Its Effect on Electrocatalytic Activity *(submitted)* 2025

Chapter 4 : The potential-dependent structure of Pt_3Ni alloy electrocatalysts and its effect on electrocatalytic activity

4.1 Introduction

Platinum-based alloys such as Pt_3Ni are a core component of modern fuel cells, serving as the oxygen reduction reaction (ORR) catalyst on the cathode side[1–4]. Compared to pure Pt electrocatalysts used in older generations, these alloys show both higher activity and stability [5–12]. Similar improvements have been observed for other reactions, such as methanol oxidation[13,14] and hydrolytic hydrogenation[15]. The origin of these improvements can be attributed to strain and ligand effects in the alloys, which modulate the electronic structure of the active Pt surface atoms [16]. Briefly, the ligand effect [17,18] refers to the change in the electronic structure of the Pt atoms due to the proximity of the alloying metal atoms, whereas the strain effect points to the reduction of the interatomic distance of the Pt metal atoms due to the introduction of relatively smaller transition metal (e.g. Pt: 0.139 nm, Ni:0.124 nm[19]) in the matrix, causing the compression of the surface atomic structure. Theoretical studies[20–23] have shown that using the strain and ligand effects, the d-band center can be shifted to a more favorable position in alloys with respect to pure Pt. This optimizes the binding strength of the reaction intermediates on the surface and thus enhances the activity[20–22].

To exploit the strain and ligand effects in electrocatalyst design, it is critical to consider the evolution of the Pt-alloy structure under electrochemical conditions. For example, for Pt-Ni alloys in acidic electrolyte, the Ni atoms leach out at the surface, leading to the formation of a pure Pt skin and a Pt-alloy core[23–25]. An inverse correlation between the ligand and strain effects and the Pt skin thickness is observed in the literature[26], with the compressive strain exerted on the surface Pt atoms as well as the electronic structure modification due to the ligand effect scale down with thicker Pt skins. Therefore, any enhancement due to ligand and strain effects, such as higher ORR activity, also depends inversely on the thickness of this Pt skin layer[16,17], making the skin layer formation properties of Pt-alloy electrocatalysts a critical design parameter [26,27].

Here, we hypothesized that the nature of the Pt skin layer in electrochemical systems may not only depend on the electrolyte pH, but also on the applied potential. This hypothesis is based on the alloy restructuring observed in heterogeneous catalysis, where elemental redistribution within the catalyst particles occurs depending on the adsorbates delivered from the gas phase. For example, in Pd-Rh alloys, it was shown that Rh is drawn to the surface in an oxidizing NO environment, whereas a Pd-Rh mixture is formed at the surface in a CO atmosphere[28]. Importantly, these effects are reversible, meaning that the particle dynamically equilibrates to its environment. Similar restructuring has been observed for Pt bimetallic catalysts in gas-phase systems when the catalyst is thermally oxidized (drawing out e.g. Ni) or reduced (bringing Pt to the surface)[23,29–31]. Here, we studied whether such reversible restructuring can also occur under electrochemical conditions, where the surface adsorbate structure is strongly dependent on the applied potential.

To observe the elemental distribution within Pt-alloy nanoparticles under electrochemical conditions, we have employed an electrochemical X-ray photoelectron spectroscopy (XPS) approach based on a graphene-covered membrane electrode assembly. Taking the example of

a Pt_3Ni alloy, we demonstrate that its structure is highly dynamic under varying applied potentials, resulting in a potential-dependent catalytic activity.

4.2 Methods

i) In situ X-ray spectroscopy

To conduct the electrochemical XPS measurements, a graphene-covered membrane electrode assembly (MEA) (Figure 4.1a) was used in an in-house designed spectro-electrochemical cell. The detailed construction of the cell, as well as the MEA has been discussed in our earlier work[32–34] and is described in detail in the supplementary information C4.1-4.6. Briefly, the MEA is made up of ~5 nm Pt_3Ni catalyst nanoparticles sputter-deposited onto a cleaned and activated Nafion membrane, and then coated with a bilayer graphene window. This graphene window is transparent for the incoming X-rays and escaping photoelectrons, permitting XPS measurements, and provides electrical contact with the catalyst. During the in situ measurements, the membrane is wetted from the back by the electrolyte (Ar-purged 0.1 M Sulfuric Acid, Sigma-Aldrich 99.9% purity). This electrolyte permeates through the proton-exchange membrane (Nafion) to the catalyst. The key function of the graphene window is to impede the evaporation of this electrolyte into the vacuum of the XPS chamber, so that XPS measurements can be conducted under wet electrochemical conditions.

To conduct the measurements, the near ambient pressure end station B-07C at Diamond Light Source, UK was utilized. The XPS signal was collected using the SPECS Phoibos NAP analyzer, whereas the total electron yield X-ray absorption spectroscopy (XAS) at the Ni L-edge was measured via the current collected on the analyzer cone. Care was taken to avoid beam damage on the Nafion membranes. Therefore, each spectrum was recorded at a new location on the MEA.

The data for XPS were processed using the CASA XPS software, and Athena was used for XAS. Details of the XPS and XAS data analysis are presented in the supplementary information C4.7.

ii) Electrochemical measurements

An Ag/AgCl reference electrode (eDAQ Leakless Miniature Ag/AgCl Reference Electrode), Pt counter electrode, and Biologic potentiostat (SP-200) were used in the XPS set-up. For reporting purposes, all the potentials mentioned in this work are converted to the RHE scale. Prior to the measurement, the potential was cycled between 0.1 V_{RHE} and 1.2 V_{RHE} at 50 mVs^{-1} to prevent any memory effects and to aid the leaching of the unstable Ni atoms from the surface layer of the bi-metallic catalyst particles[35]. For the chronoamperometry series, the potential was stepped between 0.1 V_{RHE} and 1.3 V_{RHE}.

Supporting glass cell measurements were conducted with a similar arrangement. However, the catalyst was deposited onto a polished glassy carbon disc (preparation described in the SI-C4.2) and measurements were conducted using a reversible hydrogen electrode (RHE) as a reference. All the measurements were done in a hanging meniscus configuration and the electrochemical data was *iR* corrected at 85%.

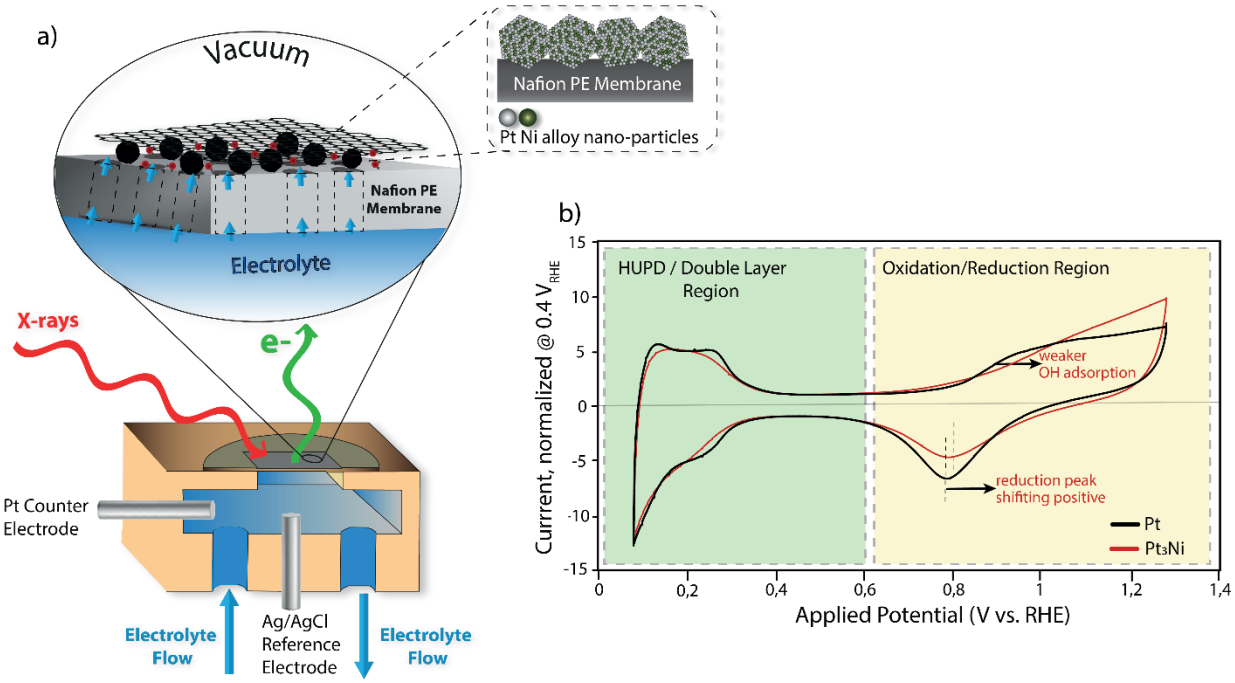

Figure 4.1: a) Cell for electrochemical XPS measurements containing an MEA consisting of the Pt_3Ni catalyst sandwiched between a Nafion membrane and a bi-layer graphene. b) Cyclic voltammograms of Pt and Pt_3Ni catalysts recorded in the XPS cell in 0.1 M H_2SO_4 at 50 mVs^{-1}, showing Hydrogen Underpotential Deposition (HUPD), Double Layer (DL) and oxidation/reduction regions

4.3 Results & Discussion

We first studied the electrochemical behavior of our Pt_3Ni catalyst. Figure 4.1b shows cyclic voltammograms (CVs) of Pt and Pt_3Ni particles recorded in the Spectro-electrochemical cell (complementary experiments in the glass cell are shown in supplementary information C4.11). The current for both curves is normalized to the double layer current at 0.4 V_{RHE} for the sake of comparison. In the oxidation region, it can be seen that the onset of oxidation, attributed to OH adsorption, is delayed for the Pt_3Ni particles compared to pure Pt, in line with the literature [36,37]. This indicates weakened adsorbate bonding, which is considered favorable for ORR because strongly bonded adsorbates function as catalyst poison in the reaction[41,42]. Other CV features frequently observed in the literature for Pt-Ni alloys, such as the PtO_x reduction peak shifting slightly positive [38,39], are also seen. Overall, these differences between Pt and Pt_3Ni highlight that Ni has a clear impact on the surface chemistry, in line with the literature[43,44].

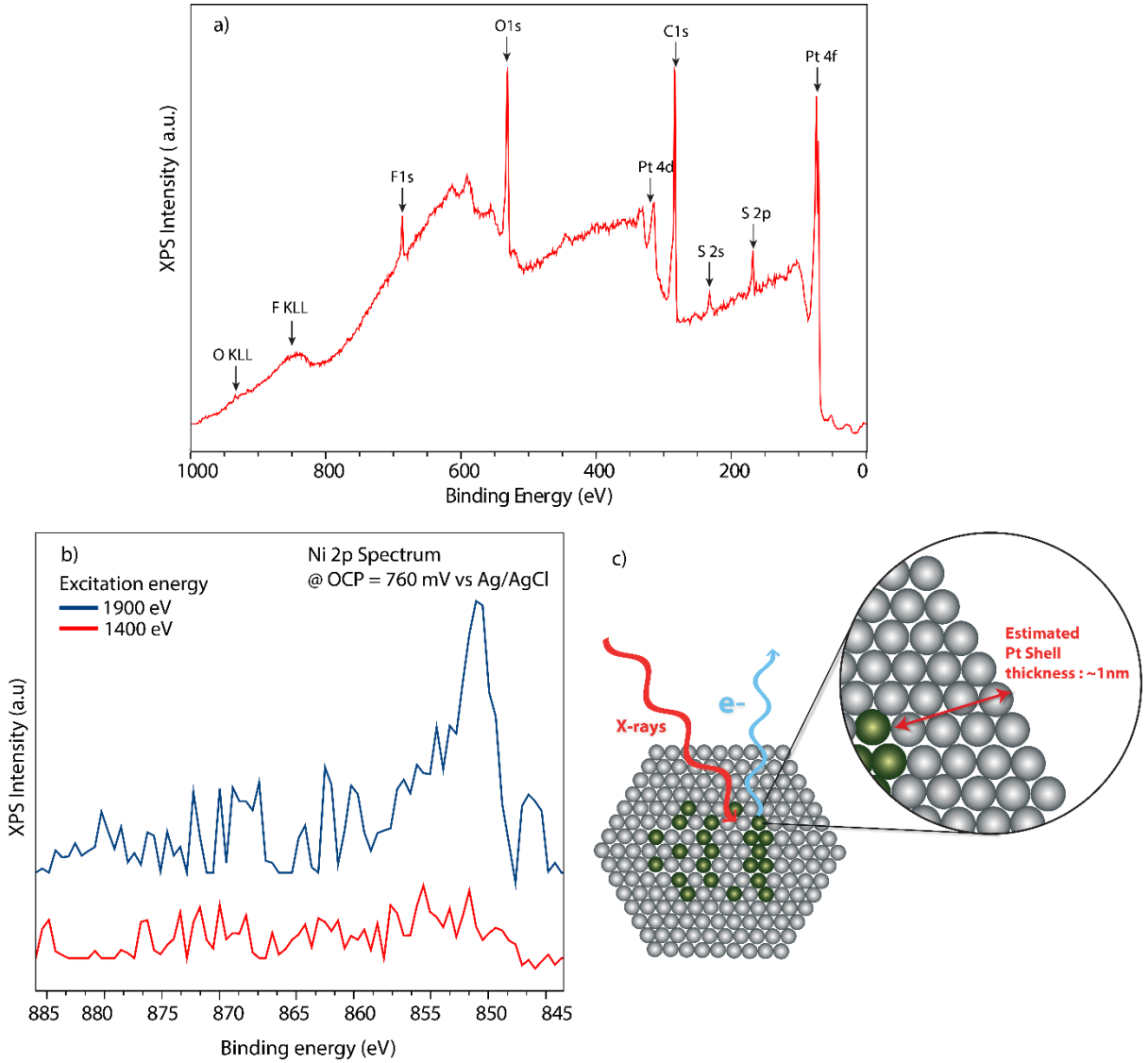

Figure 4.2 : a) Survey spectrum of OCP Pt_3Ni MEA highlighting the contributions from the membrane (S 2p, F 1s, O 1s, C 1s), graphene overlayer (C 1s), and the catalyst (Pt 4f), measured at 1400 eV, b) Ni 2p showing a noticeable Nickel contribution at a higher X-ray excitation energy (1900 eV) while almost no signal is seen at lower excitation energy (1400 eV), c) schematic impression of the in situ *structure of the Pt_3Ni nanoparticles, with an ~1 nm Pt shell and mixed Pt-Ni alloy core.*

As a next step, we studied the structure of the MEA and the Pt_3Ni particles using electrochemical XPS. Figure 4.2a shows a survey XPS spectrum recorded at open circuit potential (OCP, 760 mV vs. RHE) at hv = 1400 eV. The expected contributions from the Nafion membrane (S 2p, C 1s, O 1s and F 1s), the catalyst (Pt 4f), and the graphene window (C 1s) can be prominently seen. Notably, no Ni 2p contribution was observed at ~852-854 eV, indicative of the Ni leaching from the surface of the particles that is expected in acidic electrolyte[40–44]. Such leaching leads to the formation of a core-shell structure, with a Pt shell and an alloy core[45]. Indeed, Ni 2p spectra recorded at 1400 eV and 1900 eV (Figure 4.2b) show that for a higher probing depth (hv = 1900 eV), Ni is more clearly visible, consistent with a core-shell structure where the Ni resides in the core. Based on the intensity ratio of the two Ni 2p spectra

and the electron attenuation lengths calculated for Pt[46], the Pt shell thickness is estimated to be roughly 1 nm (Figure 4.2c). While this leached core-shell structure will contain less Ni than the initial Pt_3Ni composition, we will refer to the particles as Pt_3Ni particles for simplicity.

Following the characterization at open circuit potential, the catalyst behavior at various potentials was studied by stepping the potential down from 1.28 V_{RHE} to 0.1 V_{RHE}. In Figure 4.3, Pt 4f core levels show a steady decrease of the oxide contributions (Pt^{2+} and Pt^{4+}) until ~0.5 V_{RHE}, in line with the reduction currents observed in the CV in Figure 4.1b. The remaining $Pt^{\delta+}$ contribution was previously also observed for pure Pt and is attributed to an adsorbate-induced peak shift of the surface atoms [32].

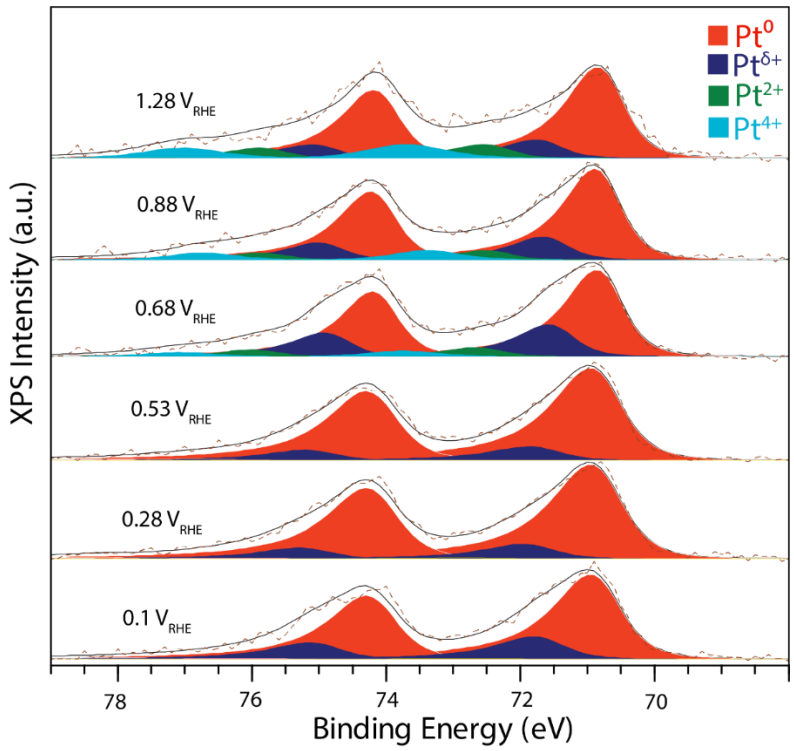

Figure 4.3: Pt 4f spectra showing the oxidation behavior of Pt in Pt_3Ni samples as a function of potential while moving from 1.28 V_{RHE} to 0.1 V_{RHE}, measured with a photon energy of 600 eV.

To track the chemistry of the Ni atoms, we recorded Ni L-edge XAS spectra within the same experiment, i.e. during the potential sequence from 1.28 V_{RHE} to 0.1 V_{RHE}. The intensity and multiplet peak pattern of the Ni L-edge are highly sensitive to the charge density of the Ni atoms, enabling the detection of even subtle changes in their electronic structure. To analyze these features, Figure 4.4 (a) displays normalized Ni L_3-edge spectra as a function of potential (normalization procedure in the supplementary information C4.10). Over the whole potential range, the spectra show a single asymmetric peak, which is typical for Ni in metal alloys [47,48]. Importantly, no extra peaks from multiplet features [49] of Ni^{2+} or Ni^{3+} oxides are observed, showing that even when the Pt shell is oxidized, all Ni remains metallic in the core. This metallic state of the Ni is also confirmed by Ni 2p spectra (supplementary information C4.12).

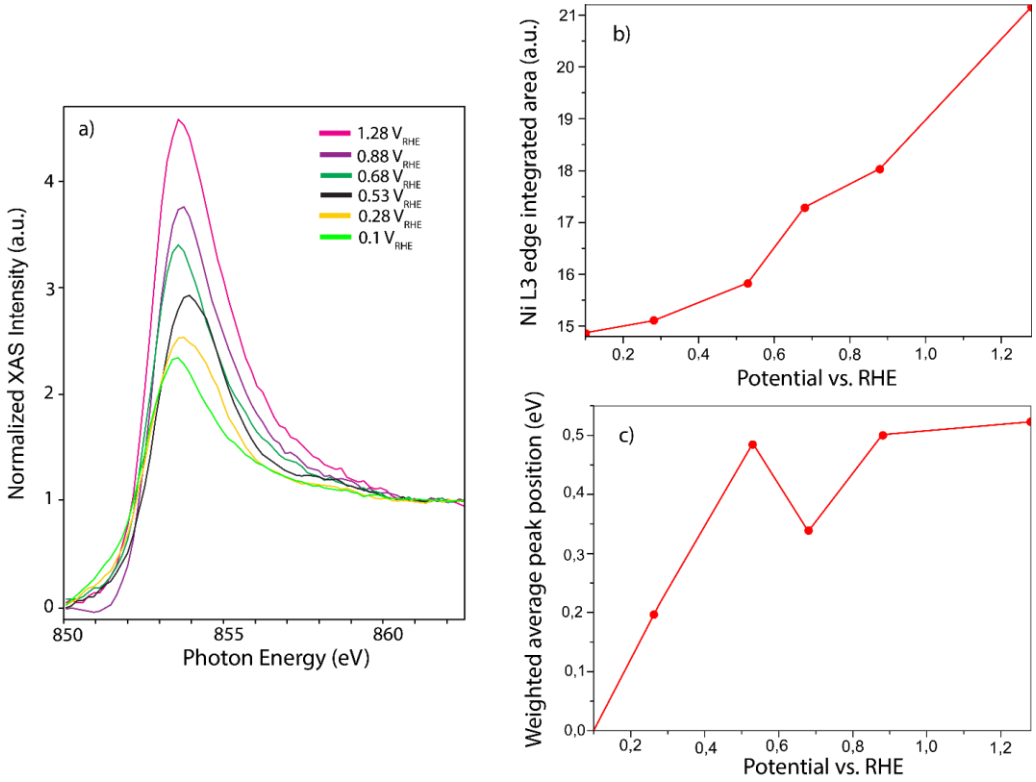

Figure 4.4: a) Ni L_3-edge spectra as a function of potential while moving from 1.28 V_{RHE} to 0.1 V_{RHE}. b) Ni L_3-edge integrated area plotted as a function of potential and c) Ni L_3-edge weighted shift in peak position plotted as a function of potential.

However, the Ni L-edge spectra do show a significant decrease in peak intensity as the potential is stepped down from 1.28 V_{RHE} to 0.1 V_{RHE}, indicating that on the more subtle level, the chemistry of the Ni atoms does change with the applied potential. Since the peak intensity in the Ni L-edge spectrum directly scales with the number of unoccupied Ni 3d states [47,50–52], the decreasing intensity indicates that the Ni d-band becomes more electron-rich as the potential is decreased. This can be rationalized based on the surface state of the particles: at low potential (<0.3 V_{RHE}), hydrogen atoms are adsorbed on the Pt shell, which do not draw much electron density from the nanoparticles. At intermediate potentials (0.3-0.6 V_{RHE}), sulfonate anions from the Nafion membrane and water molecules adsorb[53–56], which draw away slightly more electron density. Since the Ni atoms are less noble than the Pt atoms, this electron density is supplied by the Ni atoms, giving them a δ^+ state. Accordingly, a higher intensity is observed in the Ni L-edge. Above 0.6 V_{RHE}, the Pt shell is oxidized, drawing more electron density from the Ni atoms, further increasing their δ^+ character. Thus, although the Ni atoms are located in the core of the particle, they do play a role in the surface chemistry of the particles, in line with the observed Ni-induced effects in the CV (Figure 4.1b).

Figure 4.4a and c show that the peak position of the Ni L-edge is also affected by the potential-dependent chemical state of the Ni atoms. This can in part be explained by the partial oxidation of the Ni atoms to a δ^+ state: an increase Ni 3d vacancies reduces the electron-electron repulsion experienced by the Ni 2p core electrons, leading to a shift in the weighted average peak position of Ni L_3-edge to a higher energy as shown in Figure 4.4c (details of calculation of

the weighted average are presented in the supplementary information C4.10). However, a comparison of Figure 4.4b and c shows that there is a non-monotonous shift in the Ni L-edge peak position as well as a gradual broadening of the peak, which does not follow a consistent trend as the Ni L-edge intensity. Keeping in mind that the Ni L-edge peak position not only depends on the oxidation state, but also the coordination environment of the Ni atoms[57], this suggests that not only the charge density on the Ni atoms, but also their coordination environment changes.

To further investigate this potential-dependent restructuring of the particles, we studied the Ni 2p /Pt 4f peak area ratio (Figure 4.5, details of peak integration and ratio calculations in supplementary Information C4.8). This ratio provides an indication of the location of the Ni atoms: a low ratio indicates that the Ni atoms are located deeply in the core. Under these conditions, the Ni 2p signal is strongly attenuated due to scattering of the photoelectrons in the Pt shell, whereas the Pt 4f electrons in the shell can reach the electron analyzer essentially unhindered. If the Ni moves closer to the particle surface, this attenuation effect in the Ni 2p signal is decreased, resulting in a higher Ni 2p/Pt 4f ratio. This process is clearly observed in Figure 4.5, which shows that the Ni 2p/Pt 4f ratio markedly increases with increasing potential. This means that, as the adsorbates on the Pt_3Ni particles become increasingly electron-withdrawing at higher potentials, the Ni atoms are not only polarized to a δ^+ charge state, but also drawn closer to the surface. Note, however, that even at the highest potentials the Ni does not become part of the surface, as evidenced by the fact that the Ni atoms are not oxidized to Ni^{2+} at potentials where the Pt oxidizes. Hence, the migration of the Ni atoms is a subsurface event, as schematically depicted in Figure 4.5b. Importantly, the Ni migration is a reversible effect: it can be observed both when the potential is first held at 1.28 V_{RHE} and then stepped down to 0.1 V_{RHE} (red line in Figure 4.5a) and when the potential is held at 0.1 V_{RHE} and then stepped up to 1.28 V_{RHE} (black line in Figure 4.5a). Note that the offset between the two lines results from the fact that they were recorded using two different samples, with slight variation in catalyst structure.

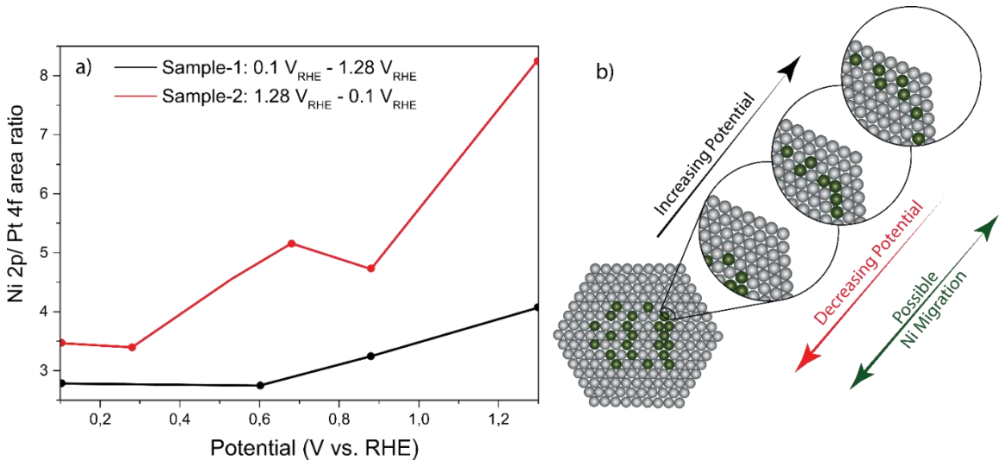

Figure 4.5: Ni location tracking via the Pt 4f/Ni 2p ratio as a function of potential and b) Pt_3Ni nanoparticle structure showing the migration of Ni towards and away from the surface as a function of potential

Chapter 4 : The potential-dependent structure of Pt_3Ni alloy electrocatalysts and its effect on electrocatalytic activity

The potential-induced migration of Ni causes the thickness of the Pt shell to vary with the applied potential. As discussed in the introduction, the Pt shell thickness has an important effect on the catalytic properties of Pt-alloys[26,27,58]. In order to probe this effect for our Pt_3Ni particles, we designed a potential step experiment where the potential was first held at either 0.3 V_{RHE} (thick Pt shell) or 0.9 V_{RHE} (thin Pt shell), followed by a switch to -0.01 V_{RHE} to measure the hydrogen evolution reaction (HER) activity of the particles. As shown in Figure 4.6, there is a marked difference between the two sequences: the HER activity following a hold at 0.9 V_{RHE} is 31% higher than after a hold at 0.3 V_{RHE}. Such a difference is not observed for pure Pt particles, confirming that the effect is caused by Ni migration. The important conclusion that can be drawn from these experiments is that the catalytic properties of Pt_3Ni electrocatalysts depend on the potential at which they are used.

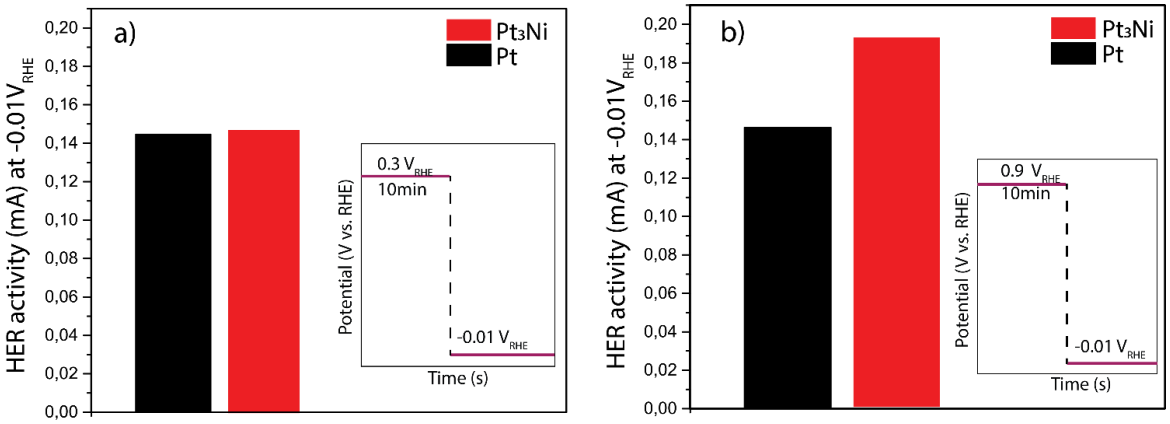

Figure 4.6: The effect of Ni migration on the hydrogen evolution reaction (HER) activity of Pt_3Ni; a) Low potential conditioning at 0.3 V_{RHE} (thick Pt shell) and b) high potential conditioning at 0.9 V_{RHE} (thin Pt shell). Pure Pt particles are shown for reference. The experiments were conducted in a glass cell in Ar-saturated 0.1 M $HClO_4$ with sputter-coated Pt_3Ni and Pt glassy carbon substrates. The HER current was averaged for 30 seconds after stabilization of the current to avoid (pseudo)capacitive contributions.

To obtain insight into the time scale of the Ni migration, the potential step experiment was repeated with different conditioning times at 0.9 V_{RHE}. As can be seen in Figure 4.7, the enhancement of the HER current stabilizes at a conditioning time of about 10 minutes. This indicates that the Ni atoms are able to move over several atomic spaces in a matter of minutes to find their equilibrium configuration at 0.9 V_{RHE}. Considering that the experiments were carried out at room temperature, this is a remarkable rate. It may therefore be hypothesized that Ni diffusion is accelerated by the adsorption-induced charge transfer from the Ni to the adsorbates, analogous to the Cabrera-Mott mechanism for metal oxide formation[59].

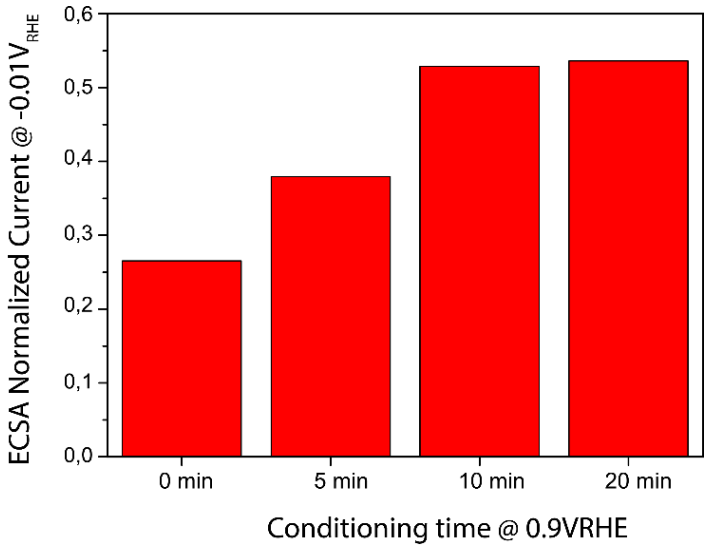

Figure 4.7: Effect of high potential (0.9 V_{RHE}) conditioning time on HER activity. The HER current here was averaged over 30 seconds and has been normalized to the case without the high potential conditioning step, to highlight the relative effect of high potential conditioning on Ni migration and the timescale on which it occurs.

4.4 Conclusions

In conclusion, we have shown that the structure and catalytic properties of Pt_3Ni nanoparticles are dependent on the applied potential. The restructuring of the particles is subtle: a $PtNi_x$ core – Pt shell structure is maintained over the entire potential range, but the thickness of the Pt shell varies due to Ni migration. Nonetheless, this restructuring has marked effect on the catalytic properties of the particles, as probed through the hydrogen evolution reaction. The driving force for the Ni migration is the interaction between the Ni atoms in the core and the adsorbates on the particle surface, which involves charge transfer from Ni to the surface. This interaction is strong enough to facilitate Ni migration on the time scale of minutes. Importantly, the adsorbate-interaction driven alloy restructuring uncovered here is a very general mechanism, that one may anticipate to occur for other alloys as well. Therefore, we expect that in situ restructuring of alloys is an important factor to consider in the design of bimetallic electrocatalysts with optimal binding properties.

References

(1) Colón-Mercado, H. R.; Popov, B. N. Stability of Platinum Based Alloy Cathode Catalysts in PEM Fuel Cells. *J Power Sources* **2006**, *155* (2), 253–263. https://doi.org/10.1016/j.jpowsour.2005.05.011.

(2) Gu, J.; Zhang, G. M.; Yao, R.; Yu, T.; Han, M. F.; Huang, R. S. High Oxygen Reduction Activity of Pt-Ni Alloy Catalyst for Proton Exchange Membrane Fuel Cells. *Catalysts* **2022**, *12* (3). https://doi.org/10.3390/catal12030250.

(3) Xu, W. C.; Zhang, Z. M.; Yang, C. H.; Zhao, K. M.; Wang, Y.; Tian, N.; Zhou, Z. Y.; Sun, S. G. Promotion Mechanism of PtCo Intermetallic Ordered Alloys in Oxygen Reduction Reaction and Its Application in Fuel Cells. *Electrochem commun* **2023**, *152*. https://doi.org/10.1016/j.elecom.2023.107516.

(4) Kozhokar, E.; Pavlets, A.; Pankov, I.; Alekseenko, A. Platinum–Nickel Electrocatalysts for a Proton-Exchange Membrane Fuel Cell Cathode: Their Synthesis, Acid Treatment, Microstructure and Electrochemical Behavior. *Energies (Basel)* **2023**, *16* (16). https://doi.org/10.3390/en16166078.

(5) Yu, W.; Porosoff, M. D.; Chen, J. G. Review of Pt-Based Bimetallic Catalysis: From Model Surfaces to Supported Catalysts. *ChemInform* **2013**, *44* (6). https://doi.org/10.1002/chin.201306180.

(6) Lonergan, W. W.; Vlachos, D. G.; Chen, J. G. Correlating Extent of Pt-Ni Bond Formation with Low-Temperature Hydrogenation of Benzene and 1,3-Butadiene over Supported Pt/Ni Bimetallic Catalysts. *J Catal* **2010**, *271* (2), 239–250. https://doi.org/10.1016/j.jcat.2010.01.019.

(7) Wang, J.; Li, B.; Yang, D.; Lv, H.; Zhang, C. Preparation Optimization and Single Cell Application of PtNi/C Octahedral Catalyst with Enhanced ORR Performance. *Electrochim Acta* **2018**, *288*, 126–133. https://doi.org/10.1016/j.electacta.2018.09.005.

(8) Begum, M.; Yurukcu, M.; Yurtsever, F.; Ergul, B.; Kariuki, N.; Myers, D. J.; Karabacak, T. Pt-Ni/WC Alloy Nanorods Arrays as ORR Catalyst for PEM Fuel Cells. *ECS Trans* **2017**, *80* (8), 919–925. https://doi.org/10.1149/08008.0919ecst.

(9) Wang, Q.; Mi, B.; Zhou, J.; Qin, Z.; Chen, Z.; Wang, H. Hollow-Structure Pt-Ni Nanoparticle Electrocatalysts for Oxygen Reduction Reaction. *Molecules* **2022**, *27* (8). https://doi.org/10.3390/molecules27082524.

(10) Ye, S. H.; Feng, J. X.; Wang, A. L.; Xu, H.; Li, G. R. Multi-Layered Pt/Ni Nanotube Arrays with Enhanced Catalytic Performance for Methanol Electrooxidation. *J Mater Chem A Mater* **2015**, *3* (46), 23201–23206. https://doi.org/10.1039/c5ta07098h.

(11) Navarro, R. M.; Pawelec, B.; Trejo, J. M.; Mariscal, R.; Fierro, J. L. G. *Hydrogenation of Aromatics on Sulfur-Resistant PtPd Bimetallic Catalysts*; 2000; Vol. 189. http://www.idealibrary.comon.

(12) Jia, Q.; Lewis, A.; Grice, C.; Smotkin, S.; Segre, U. In Situ XAFS Studies of the Oxygen Reduction Reaction on Carbon Supported Pt and PtNi(1:1) Catalysts. *J Phys Conf Ser* **2009**, *190*. https://doi.org/10.1088/1742-6596/190/1/012157.

(13) Zhou, Y. Y.; Liu, C. H.; Liu, J.; Cai, X. L.; Lu, Y.; Zhang, H.; Sun, X. H.; Wang, S. D. Self-Decoration of PtNi Alloy Nanoparticles on Multiwalled Carbon Nanotubes for Highly Efficient Methanol Electro-Oxidation. *Nanomicro Lett* **2016**, *8* (4), 371–380. https://doi.org/10.1007/s40820-016-0096-2.

(14) Qiu, H.; Zou, F. Nanoporous PtCo Surface Alloy Architecture with Enhanced Properties for Methanol Electrooxidation. *ACS Appl Mater Interfaces* **2012**, *4* (3), 1404–1410. https://doi.org/10.1021/am201659n.

(15) Liang, G.; He, L.; Arai, M.; Zhao, F. The Pt-Enriched PtNi Alloy Surface and Its Excellent Catalytic Performance in Hydrolytic Hydrogenation of Cellulose. *ChemSusChem* **2014**, *7* (5), 1415–1421. https://doi.org/10.1002/cssc.201301204.

(16) Shao, M.; Odell, J. H.; Peles, A.; Su, D. The Role of Transition Metals in the Catalytic Activity of Pt Alloys: Quantification of Strain and Ligand Effects. *Chemical Communications* **2014**, *50* (17), 2173–2176. https://doi.org/10.1039/c3cc47341d.

(17) Adzic, R. R.; Zhang, J.; Sasaki, K.; Vukmirovic, M. B.; Shao, M.; Wang, J. X.; Nilekar, A. U.; Mavrikakis, M.; Valerio, J. A.; Uribe, F. Platinum Monolayer Fuel Cell Electrocatalysts. *Top Catal* **2007**, *46* (3–4), 249–262. https://doi.org/10.1007/s11244-007-9003-x.

(18) Hammer, B.; Nørskov, J. K. Theoretical Surface Science and Catalysis-Calculations and Concepts; 2000; Vol. 45, pp 71–128.

(19) Callister, W. D.; David Rethwisch, J. G. *MATERIALS SCIENCE and ENGINEERING*, 9th Edition.; Sayre, D.; Wiley, pp 691–699.

(20) Stamenkovic, V. R.; Strmcnik, D.; Lopes, P. P.; Markovic, N. M. Energy and Fuels from Electrochemical Interfaces. *Nature Materials*. Nature Publishing Group December 20, 2016, pp 57–69. https://doi.org/10.1038/nmat4738.

(21) Stephens, I. E. L.; Bondarenko, A. S.; Perez-Alonso, F. J.; Calle-Vallejo, F.; Bech, L.; Johansson, T. P.; Jepsen, A. K.; Frydendal, R.; Knudsen, B. P.; Rossmeisl, J.; Chorkendorff, I. Tuning the Activity of Pt(111) for Oxygen Electroreduction by Subsurface Alloying. *J Am Chem Soc* **2011**, *133* (14), 5485–5491. https://doi.org/10.1021/ja111690g.

(22) Stamenkovic, V. R.; Mun, B. S.; Mayrhofer, K. J. J.; Ross, P. N.; Markovic, N. M. Effect of Surface Composition on Electronic Structure, Stability, and Electrocatalytic Properties of Pt-Transition Metal Alloys: Pt-Skin versus Pt-Skeleton Surfaces. *J Am Chem Soc* **2006**, *128* (27), 8813–8819. https://doi.org/10.1021/ja0600476.

(23) Lim, C.; Fairhurst, A. R.; Ransom, B. J.; Haering, D.; Stamenkovic, V. R. Role of Transition Metals in Pt Alloy Catalysts for the Oxygen Reduction Reaction. *ACS Catalysis*. American Chemical Society November 17, 2023, pp 14874–14893. https://doi.org/10.1021/acscatal.3c03321.

(24) Stamenkovic, V. R.; Mun, B. S.; Arenz, M.; Mayrhofer, K. J. J.; Lucas, C. A.; Wang, G.; Ross, P. N.; Markovic, N. M. Trends in Electrocatalysis on Extended and Nanoscale Pt-Bimetallic Alloy Surfaces. *Nat Mater* **2007**, *6* (3), 241–247. https://doi.org/10.1038/nmat1840.

(25) Bogar, M.; Yakovlev, Y.; Sandbeck, D. J. S.; Cherevko, S.; Matolínová, I.; Amenitsch, H.; Khalakhan, I. Interplay among Dealloying, Ostwald Ripening, and Coalescence in PtXNi100-XBimetallic Alloys under Fuel-Cell-Related Conditions. *ACS Catal* **2021**, *11* (18), 11360–11370. https://doi.org/10.1021/acscatal.1c01111.

(26) Morris, A. R.; Skoglund, M. D.; Holles, J. H. Characterization of Ni@Pt and Co@Pt Overlayer Catalysts Using XAS Studies. *Appl Catal A Gen* **2015**, *489*, 98–110. https://doi.org/10.1016/j.apcata.2014.10.019.

(27) Schlapka, A.; Lischka, M.; Groß, A.; Käsberger, U.; Jakob, P. Surface Strain versus Substrate Interaction in Heteroepitaxial Metal Layers: Pt on Ru(0001). *Phys Rev Lett* **2003**, *91* (1), 016101/1-016101/4. https://doi.org/10.1103/PhysRevLett.91.016101.

(28) Tao, F.; Grass, M. E.; Zhang, Y.; Butcher, D. R.; Aksoy, F.; Aloni, S.; Altoe, V.; Alayoglu, S.; Renzas, J. R.; Tsung, C. K.; Zhu, Z.; Liu, Z.; Salmeron, M.; Somorjai, G. A. Evolution of Structure and Chemistry of Bimetallic Nanoparticle Catalysts under Reaction Conditions. *J Am Chem Soc* **2010**, *132* (25), 8697–8703. https://doi.org/10.1021/ja101502t.

(29) Khalakhan, I.; Bogar, M.; Vorokhta, M.; Kúš, P.; Yakovlev, Y.; Dopita, M.; Sandbeck, D. J. S.; Cherevko, S.; Matolínová, I.; Amenitsch, H. Evolution of the PtNi Bimetallic Alloy Fuel Cell Catalyst under Simulated Operational Conditions. *ACS Appl Mater Interfaces* **2020**, *12* (15), 17602–17610. https://doi.org/10.1021/acsami.0c02083.

(30) Xie, X.; Sandhya, A. L. M.; Piliai, L.; Vorokhta, M.; Matolínová, I.; Khalakhan, I. Surface Compositional Dynamics in a PtNi Bimetallic Alloy under Simulated Operational Conditions: Electrochemical and NAP-XPS Study. *Appl Catal B* **2023**, *325*. https://doi.org/10.1016/j.apcatb.2022.122328.

(31) Ruban, A. V.; Skriver, H. L.; Nørskov, J. K. Surface Segregation Energies in Transition-Metal Alloys. *Phys Rev B Condens Matter Mater Phys* **1999**, *59* (24), 15990–16000. https://doi.org/10.1103/PhysRevB.59.15990.

(32) Javed, H.; Knop-Gericke, A.; Mom, R. V. Structural Model for Transient Pt Oxidation during Fuel Cell Start-up Using Electrochemical X-Ray Photoelectron Spectroscopy. *ACS Appl Mater Interfaces* **2022**, *14* (31), 36238–36245. https://doi.org/10.1021/acsami.2c09249.

(33) Mom, R.; Frevel, L.; Velasco-Vélez, J. J.; Plodinec, M.; Knop-Gericke, A.; Schlögl, R. The Oxidation of Platinum under Wet Conditions Observed by Electrochemical X-Ray Photoelectron Spectroscopy. *J Am Chem Soc* **2019**, *141* (16), 6537–6544. https://doi.org/10.1021/jacs.8b12284.

(34) Frevel, L. J.; Mom, R.; Velasco-Vélez, J. J.; Plodinec, M.; Knop-Gericke, A.; Schlögl, R.; Jones, T. E. In Situ X-Ray Spectroscopy of the Electrochemical Development of Iridium Nanoparticles in Confined Electrolyte. *Journal of Physical Chemistry C* **2019**, *123* (14), 9146–9152. https://doi.org/10.1021/acs.jpcc.9b00731.

(35) Glüsen, A.; Dionigi, F.; Paciok, P.; Heggen, M.; Müller, M.; Gan, L.; Strasser, P.; Dunin-Borkowski, R. E.; Stolten, D. Dealloyed PtNi-Core-Shell Nanocatalysts Enable Significant Lowering of Pt Electrode Content in Direct Methanol Fuel Cells. *ACS Catal* **2019**, *9* (5), 3764–3772. https://doi.org/10.1021/acscatal.8b04883.

(36) Matanovic, I.; Garzon, F. H.; Henson, N. J. Theoretical Study of Electrochemical Processes on Novel Platinum Group Metal Catalysts. *ACS National Meeting Book of Abstracts* **2011**, 10640–10650. https://doi.org/10.1149/ma2011-02/16/1004.

(37) Wang, J.; Li, B.; Yang, D.; Lv, H.; Zhang, C. Preparation Optimization and Single Cell Application of PtNi/C Octahedral Catalyst with Enhanced ORR Performance. *Electrochim Acta* **2018**, *288*, 126–133. https://doi.org/10.1016/j.electacta.2018.09.005.

(38) Stamenković, V.; Schmidt, T. J.; Ross, P. N.; Marković, N. M. Surface Segregation Effects in Electrocatalysis: Kinetics of Oxygen Reduction Reaction on Polycrystalline Pt3Ni Alloy Surfaces. *Journal of Electroanalytical Chemistry* **2003**, *554–555* (1), 191–199. https://doi.org/10.1016/S0022-0728(03)00177-3.

(39) Bunch, J. S.; Van Der Zande, A. M.; Verbridge, S. S.; Frank, I. W.; Tanenbaum, D. M.; Parpia, J. M.; Craighead, H. G.; McEuen, P. L. Improved Oxygen Reduction Activity on Pt3Ni(111) via Increased Surface Site Availability. *Science (1979)* **2007**, *315* (5811), 490–493. https://doi.org/10.1126/science.1136836.

(40) Wang, C.; Van Der Vliet, D.; Chang, K. C.; You, H.; Strmcnik, D.; Schlueter, J. A.; Markovic, N. M.; Stamenkovic, V. R. Monodisperse Pt3Co Nanoparticles as a Catalyst for the Oxygen Reduction Reaction: Size-Dependent Activity. *Journal of Physical Chemistry C* **2009**, *113* (45), 19365–19368. https://doi.org/10.1021/jp908203p.

(41) Patrick, B.; Ham, H. C.; Shao-Horn, Y.; Allard, L. F.; Hwang, G. S.; Ferreira, P. J. Atomic Structure and Composition of "Pt3Co" Nanocatalysts in Fuel Cells: An Aberration-Corrected STEM HAADF Study. *Chemistry of Materials* **2013**, *25* (4), 530–535. https://doi.org/10.1021/cm3029164.

(42) Mukerjee, S.; Srinivasan, S. *Enhanced Electrocatalysis of Oxygen Reduction on Platinum Alloys in Proton Exchange Membrane Fuel Cells **; Elsevier Sequoia S.A, 1993; Vol. 357.

(43) Huang, Y.; Zhang, J.; Kongkanand, A.; Wagner, F. T.; Li, J. C. M.; Jorné, J. Transient Platinum Oxide Formation and Oxygen Reduction on Carbon-Supported Platinum and Platinum-Cobalt Alloy Electrocatalysts. *J Electrochem Soc* **2014**, *161* (1), F10–F15. https://doi.org/10.1149/2.018401jes.

(44) Zhang, K.; Yue, Q.; Chen, G.; Zhai, Y.; Wang, L.; Wang, H.; Zhao, J.; Liu, J.; Jia, J.; Li, H. Effects of Acid Treatment of Pt-Ni Alloy Nanoparticles@graphene on the Kinetics of the Oxygen Reduction Reaction in Acidic and Alkaline Solutions. *Journal of Physical Chemistry C* **2011**, *115* (2), 379–389. https://doi.org/10.1021/jp108305v.

(45) Markovic, N.; Browning, A.; Stamenkovic, V.; Roy, J.; Grunder, Y.; Thompson, P.; Fowler, B.; Lucas, C. From Ultra-High Vacuum to the Electrochemical Interface: X-Ray Scattering Studies of Model Electrocatalysts. *Faraday Discussions*. 2008, pp 9–10. https://doi.org/10.1039/b814058h.

(46) Cumpson, P. J.; Seah, M. P. Elastic Scattering Corrections in AES and XPS. II. Estimating Attenuation Lengths and Conditions Required for Their Valid Use in Overlayer/Substrate Experiments. *Surface and Interface Analysis* **1997**, *25* (6), 430–446. https://doi.org/10.1002/(SICI)1096-9918(199706)25:6<430::AID-SIA254>3.0.CO;2-7.

(47) Chang, Y. K.; Lin, K. P.; Pong, W. F.; Tsai, M. H.; Hseih, H. H.; Pieh, J. Y.; Tseng, P. K.; Lee, J. F.; Hsu, L. S. Charge Transfer and Hybridization Effects in Ni3Al and Ni3Ga Studies by X-Ray-Absorption Spectroscopy and Theoretical Calculations. *J Appl Phys* **2000**, *87* (3), 1312–1317. https://doi.org/10.1063/1.372015.

(48) Van Der Laan, G.; Thole, B. T.; Sawatzky, G. A.; Verdaguer, M. *Multiplet Structure in the L2,3 x-Ray-Absorption Spectra: A Fingerprint for High-and Low-Spin Ni Compounds*; Vol. 37.

(49) Regan, T. J.; Ohldag, H.; Stamm, C.; Nolting, F.; Lüning, J.; Stöhr, J.; White, R. L. Chemical Effects at Metal/Oxide Interfaces Studied by x-Ray-Absorption Spectroscopy. *Phys Rev B Condens Matter Mater Phys* **2001**, *64* (21). https://doi.org/10.1103/PhysRevB.64.214422.

(50) Kasatikov, S.; Fantin, A.; Manzoni, A. M.; Sakhonenkov, S.; Makarova, A.; Smirnov, D.; Filatova, E. O.; Schumacher, G. *Chemical Interaction and Electronic Structure in a Compositionally Complex Alloy: A Case Study by Means of X-Ray Absorption and X-Ray Photoelectron Spectroscopy*.

(51) Hsieh, H. H.; Chang, Y. K.; Pong, W. F.; Pieh, J. Y.; Tseng, P. K.; Sham, T. K.; Coulthard, I.; Naftel, S. J.; Lee, J. F.; Chung, S. C.; Tsang, K. L. *Electronic Structure of Ni-Cu Alloys: The d-Electron Charge Distribution*; 1998.

(52) Mukerjee, S.; Srinivasan, S.; Soriaga, M. P. Role of Structural and Electronic Properties of Pt and Pt Alloys on Electrocatalysis of Oxygen Reduction: An In Situ XANES and EXAFS Investigation. *J. Electrochem. Soc* **1995**, *142*, 1409.

(53) Su, Z.; Climent, V.; Leitch, J.; Zamlynny, V.; Feliu, J. M.; Lipkowski, J. Quantitative SNIFTIRS Studies of (Bi)Sulfate Adsorption at the Pt(111) Electrode Surface. *Physical Chemistry Chemical Physics* **2010**, *12* (46), 15231–15239. https://doi.org/10.1039/c0cp00860e.

(54) Kolics, A.; Wieckowski, A. Adsorption of Bisulfate and Sulfate Anions on a Pt(111) Electrode. *Journal of Physical Chemistry B* **2001**, *105* (13), 2588–2595. https://doi.org/10.1021/jp003536f.

(55) Teliska, M.; Murthi, V. S.; Mukerjee, S.; Ramaker, D. E. Site-Specific vs Specific Adsorption of Anions on Pt and Pt-Based Alloys. *Journal of Physical Chemistry C* **2007**, *111* (26), 9267–9274. https://doi.org/10.1021/jp071106k.

(56) Yano, H.; Uematsu, T.; Omura, J.; Watanabe, M.; Uchida, H. Effect of Adsorption of Sulfate Anions on the Activities for Oxygen Reduction Reaction on Nafion®-Coated Pt/Carbon Black Catalysts at Practical Temperatures. *Journal of Electroanalytical Chemistry* **2015**, *747*, 91–96. https://doi.org/10.1016/j.jelechem.2015.04.007.

(57) Chen, J.; Finfrock, Y. Z.; Wang, Z.; Sham, T. K. Strain and Ligand Effects in Pt-Ni Alloys Studied by Valence-to-Core X-Ray Emission Spectroscopy. *Sci Rep* **2021**, *11* (1). https://doi.org/10.1038/s41598-021-93068-0.

(58) Strasser, P.; Koh, S.; Anniyev, T.; Greeley, J.; More, K.; Yu, C.; Liu, Z.; Kaya, S.; Nordlund, D.; Ogasawara, H.; Toney, M. F.; Nilsson, A. Lattice-Strain Control of the Activity in Dealloyed Core-Shell Fuel Cell Catalysts. *Nat Chem* **2010**, *2* (6), 454–460. https://doi.org/10.1038/nchem.623.

(59) Cabrera, N.; Mott, N. F. Theory of the Oxidation of Metals. *Reports on Progress in Physics* **1949**, *12* (1), 163–184. https://doi.org/10.1088/0034-4885/12/1/308.